C. R. Chimie 22 (2019) 761–770

Contents lists available at ScienceDirect

Comptes Rendus Chimie

www.sciencedirect.com

Preliminary communication/Communication

The synthesis of sulphonated hypercrosslinked exchange resin for free fatty acid esterification

Nurul Asmawati Roslan [a], Norhayati Abdullah [a], Sumaiya Zainal Abidin [a, b, *]

[a] Faculty of Chemical and Process Engineering Technology, College of Engineering Technology, Universiti Malaysia Pahang, Lebuhraya Tun Razak, 26300 Gambang, Pahang, Malaysia
[b] Centre of Excellence for Advanced Research in Fluid Flow (CARIFF), Universiti Malaysia Pahang, Lebuhraya Tun Razak, 26300 Gambang, Pahang, Malaysia

ARTICLE INFO

Article history:
Received 31 May 2019
Accepted 26 August 2019
Available online 3 October 2019

Keywords:
Esterification
Free fatty acid
Used cooking oil
Ion-exchange resin
Catalyst

ABSTRACT

Esterification has been extensively used as a pretreatment process in biodiesel production to reduce the free fatty acid (FFA) content in the feedstock. This study investigates the potential of sulphonated hypercrosslinked exchange resin (SHER), a newly synthesised catalyst for the esterification reaction. The experimental works were divided into two stages: (1) the synthesis and characterisation of the catalyst and (2) screening study on the esterification of FFAs in used cooking oil (UCO) using different types of ion-exchange resins. SHER was found to have excellent characteristics with high specific surface area (~836 m^2 g^{-1}) and thermal decomposition temperature (398 °C). The SHER was then subjected to the esterification reaction and outperformed other catalysts with 90% FFA conversion followed by Diaion RCP145H, SK1BH and PK228LH. The excellent catalytic performance of SHER is due to the high specific surface area that allows FFA molecules to easily access their active sites.

1. Introduction

Nowadays, research into biodiesel as a sustainable alternative fuel has been widely investigated around the world. Biodiesel can be synthesised from vegetable oils or animal fats. It is an attractive alternative fuel for fossil diesel engine because of its renewability, biodegradability and nontoxicity [1,2]. It also has the potential to reduce pollutants originated from vehicle emissions and has been proven to have good combustion properties [3,4]. Besides that, biodiesel can be directly used in the existing fossil diesel infrastructure.

Transesterification reaction is one of the well-known methods that can be used to produce biodiesel [5]. It is a reaction between vegetable oils or other fats and an alcohol with or without the presence of a catalyst. Traditionally, refined vegetable oils such as soybean oil, sunflower oil and palm oil are used as feedstocks to synthesise biodiesel. However, the cost of feedstocks accounts for more than 75% of the biodiesel production cost [6,7]. High production cost has become a major challenge in scaling up the biodiesel production and widespread use of biodiesel. Apart from that, the usage of edible oils as the feedstock is not practical because of the high competition with the food industry. Thus, the utilisation of a cheaper feedstock [i.e. nonedible used cooking oil (UCO)] which is readily available, cheaper and environmentally friendly has been investigated widely today. It is found to be an attractive and effective feedstock to synthesise biodiesel and thus reduces the total production cost [8,9].

However, the direct usage of nonedible oils leads to several problems such as incomplete recovery of the catalysts, low biodiesel yield and high purification cost. This is due to the significant presence of free fatty acid (FFA), thus

* Corresponding author. Faculty of Chemical and Process Engineering Technology, College of Engineering Technology, Universiti Malaysia Pahang, Lebuhraya Tun Razak, 26300 Gambang, Pahang, Malaysia.
E-mail address: sumaiya@ump.edu.my (S.Z. Abidin).

https://doi.org/10.1016/j.crci.2019.08.004
1631-0748/

making the synthesis process of biodiesel becomes complicated [10]. High contents of FFAs and water in UCO lead to saponification reaction [11]. The saponification reaction is a result of interaction between FFAs and water which inhibits the separation process of esters from glycerol and reduces the biodiesel yield [12]. To address this, a pretreatment stage, which is also known as esterification process, is introduced by several researchers to reduce the FFA content before the mixture is further subjected to transesterification reaction to convert the remaining fatty acids into biodiesel [13–15]. In the esterification reaction, sulphuric acid was commonly used as a catalyst because of its low cost, but the usage leads to several drawbacks such as equipment corrosion, effluent disposal problems, slow reaction rate, and difficulty in catalyst recovery due to the similar homogeneity between the catalyst and products [16]. These drawbacks have led to studies on heterogeneous solid acid catalysts such as zeolites [17], alumina [18] and ion-exchange resins [19–22] in the esterification reaction.

In esterification reaction, a cation-exchange resin grafted with a sulphonic group is frequently used as a catalyst because of its acidic characteristic. Ion-exchange resin is preferable because it is noncorrosive, insensitive to FFAs, and able to catalyse the reaction under mild reaction conditions [23–25]. Fu et al. [19] investigated the performance of ion-exchange resins as a catalyst in the FFA esterification. Owing to the high porosity and accessible acid sites of the catalyst, 97.8% of FFA conversion was achieved during the reaction. A study of the different matrix types of cation-exchange resins was also conducted by Feng et al. [26]. Three types of resins were used in this study, namely, NKC-9 (macroreticular), 001 × 7 (gelular) and D61 (macroreticular). In contrast, the highest FFA conversion was obtained using NKC-9, and this resin also showed a good conversion in the reusability study. However, the conventional ion-exchange resin has low acidic sites, low porosity which leads to the moderate surface area, low degradation temperature (i.e. maximum 120 °C); is capable of losing activity under harsh conditions and requires longer reaction time [27,28]. Ion-exchange resin with a high specific surface area and acidity is required to increase the active sites of the catalyst which helps to increase the FFA conversion and speeds up the reaction. Besides that, resin with high thermal stability is needed to catalyse the reaction at higher temperature while maintaining the active site of the catalyst. Functionalised hypercrosslinked polymer as a new ion-exchange resin has been widely investigated today. The attachment of the functional groups to polymers is the first step towards the preparation of functional polymers for specific uses. It has demonstrated a good performance as a porous material because they have high specific surface area and good thermal stability [29,30]. Besides that, the functionalisation of the hypercrosslinked polymer can be modified depending on the application. These advantages make the versatile hypercrosslinked polymer a viable alternative to be applied in the esterification reaction. The preparation of functionalised hypercrosslinked polymer is significant and challenging mainly in maintaining the right technique to ensure the quality of the catalyst produced. Hypercrosslinked polymer is a new generation of polymer which is synthesised by extensive postcrosslinking of polymer chains. The properties of this polymer are enhanced because of the introduction of numerous methylene bridges between aromatic rings [31]. The products obtained by this technique are conformationally rigid, display high specific surface areas, able to sorb polar and nonpolar solvents and are characterised by an exceptionally rigid open-network structure of high permeability [32]. However, till date, there is no utilisation of this type of hypercrosslinked polymer as a catalyst in the esterification reaction of UCO.

Hence, the present work focuses on the production of a hypercrosslinked particle to be used as a catalyst in the esterification reaction. The first stage of the study focuses on the synthesis and characterisation of the sulphonated hypercrosslinked exchange resin (SHER), and the second stage investigates the performance of few cation-exchange resins including SHER in the FFA esterification. In the first stage, three main steps are involved in the preparation of SHER: (a) preparation of precursor, (b) preparation of hypercrosslinked beads and (c) sulphonation of the hypercrosslinked beads. The samples were subjected to different characterisation methods such as the N_2 physisorption via the Brunauer–Emmett–Teller (BET) method, particle size distribution (PSD), X-ray fluorescence (XRF), thermal gravimetric analysis (TGA), scanning electron microscopy (SEM), Fourier-transform infrared (FTIR), ion-exchange capacity (IEC) and elemental analysis (C, H, N, and S). The second stage investigated the potential of the functionalised hypercrosslinked polymer as a catalyst in FFA esterification using simulated UCO as the feedstock.

2. Methodology

2.1. Stage 1: synthesis of SHER

There are three main stages in the preparation of SHER: the preparation of precursor/nonaqueous dispersion (NAD) particles, the preparation of hypercrosslinked beads by hypercrosslinking reaction and the sulphonation of hypercrosslinked particles. Few variables were varied at each stage to obtain the best resin to be used in the esterification reaction. In preparing the NAD particles, styrene (St) (99%) acted as a monomer, vinylbenzyl chloride (VBC) (95%) as a comonomer, poly (*N*-vinylpyrrolidone) (PVP)-55 (M_w ~ 55,000) as a stabiliser, Triton X-305 (99%) as a costabiliser, benzoyl peroxide (BPO) (95%) as an initiator and ethylene glycol dimethacrylate (EGDMA) (98%) as a cross-linker.

First, the precursor particles were synthesised by the NAD technique. St, VBC, ethanol, PVP-55, Triton X-305 and BPO were mixed in a round-bottomed flask (i.e. polymerisation vessel) fitted with a nitrogen (N_2) inlet, condenser and overhead stirrer. The mixing process was conducted at room temperature, and once a homogeneous solution formed, the solution was bubbled for 30 min with the N_2 gas. The flask was then placed on a heating mantle at 70 °C, and the solution was stirred at 120 rpm for 1 h. This step is known as the polymerisation step. In a separate flask, a solution containing EGDMA was prepared and heated up to 70 °C under the flow of nitrogen. When the temperature reached 70 °C, the hot solution was added dropwise into

the polymerisation vessel. The solution was continuously heated and stirred for the next 23 h. The resulted slurry mixture was subsequently introduced to a centrifuge for phase separation. The process took about 20 min (i.e. 10 min with ethanol and 10 min with methanol) at 3000 rpm, resulting two layers of solid and liquid. The forming particles, known as NAD particles, were filtered and dried at 40 °C for 12 h. In this step, the concentration of St (50–90%), VBC (10–50%) and EGDMA (0.5–1.5 wt%) was varied to obtain the best shape of the precursor (NAD) particles.

For the hypercrosslinked bead preparation, 1.2 g of the NAD particles was added to 40 mL of 1,2-dichloroethane (DCE) (99%) solvent. Under the flow of N_2, they were then left for 1 h to let the NAD particle to swell. Ferric chloride ($FeCl_3$) which acts as a catalyst was added into the reaction flask. The precursor particle was hypercrosslinked by this $FeCl_3$. The mixture was then heated immediately at 80 °C for 18 h. The forming particles were recovered using the centrifugation process operated at 3000 rpm for 10 min, producing two separate layers. The solid particles were recovered by the filtration method. The particles were washed with methanol and aqueous nitric acid to remove impurities. Then, the beads were extracted with acetone for 12 h. The particles were then washed few times with methanol before being dried at 40 °C overnight. In this step, different loading of Lewis acid catalyst ($FeCl_3$, 99%) (i.e. 0.5:1, 1:1 and 1.5:1) was tested to produce hypercrosslinked beads with a high specific surface area.

In the sulphonation procedure, the hypercrosslinked beads were charged into a flask containing anhydrous DCE (30 mL). Then, N_2 was let to flow into the flask. The mixture was left in the flask to wet the beads for 1 h. After that, sulphuric acid was added and heated up to 60 °C with continuous mechanical stirring. The particles were allowed to cool in an ice-water bath after 18 h (reaction time) to quench the reaction, followed by washing process until the pH of the filtrate became neutral. The solution was subsequently filtered using a vacuum filtration system. The particles were dried overnight at 40 °C. In this step, the sulphonation reagent was varied from 1 to 5 wt% to obtain the best beads in terms of the specific surface area before the esterification reaction. The method of synthesis of SHER is summarised in a graphical form in the Supplementary file.

2.2. Characterisation analysis

The specific surface area of the ion-exchange resins was measured by N_2 physisorption analysis using the Micromeritics ASAP 2000 porosimeter. To determine the percentage content of carbon (C), hydrogen (H), nitrogen (N) and sulphur (S) in the resin, an analyser (Elementar, Germany) was used. IEC was calculated by the titration method. PSD was carried out using a Malvern Mastersizer 2000 to measure the distribution pattern of the catalysts. The TGA was performed via a thermogravimetric analyser (Q500) to determine the degradation temperature and decomposition point of the catalyst. The surface morphology of catalysts was analysed by SEM (CARL ZEISS). To monitor the chlorine content in the precursor beads, XRF analysis (S8 Tiger; Bruker) was performed. The detailed description on the characterisation techniques is provided in the Supplementary file.

2.3. Stage 2: esterification of FFAs in highly acidified oil using ion-exchange resins as catalysts

a) Preparation of simulated used cooking oil

Virgin palm oil and oleic acid were mixed to prepare the simulated used cooking oil (SUCO) with 6% of FFA content. The solution was mixed in a conical flask and stirred until the solution becomes homogeneous. The acid value of the prepared SUCO was approximately 12 mg KOH g^{-1}.

b) Preparation of the commercialised catalyst

Diaion catalysts (RCP145H, SK104H and PK208LH) were provided by Mitsubishi Chemical Corporation. First, all the wet resins were immersed overnight in methanol. Then, the resins together with methanol were ultrasonicated for about 9–10 times until the colour of methanol changed from light brown to colourless. This method was carried out to ensure all the contaminants were removed. The conductivity value of the residual solution was recorded in each washing cycle until it was approximately the same as the conductivity of the solvent (methanol), which was 0.23 μS m^{-1}. All the resins were finally placed in the oven for 6 h at 100 °C to remove water and remaining methanol.

c) Esterification of FFAs in SUCO

The reactions were carried out in a 500-ml four-neck round-bottomed flask. The reaction temperature was set at 60 °C and controlled using a programmable temperature controller. Methanol and SUCO were first added to the reaction flask, and the solution was heated and stirred until the desired reaction temperature was reached. Then, 1.5 wt % of the catalyst was added to the reaction mixture, and after the catalyst addition, the first sample was taken for FFA analysis. This time was recorded as the initial reaction time. The samples were taken periodically at specified time intervals, and the reaction lasted for 8 h. The reaction conditions of 1.5 wt% of catalyst loading, 60 °C, 12:1 of methanol-to-SUCO feed molar ratio and 150 rpm were kept constant for all catalysts.

d) Acid number and FFA content

The acid number of the sample was determined by the ASTM D974 standard method. Initially, two grams of the sample was taken and weighted. The sample was then dissolved in a titration solvent. The titration solvent was prepared by mixing 2-propanol, toluene and water. The mixture was titrated using potassium hydroxide solution and α-naphtholbenzein as an indicator. The acid number was calculated using Eq. 1:

$$N_{acid} = 56.1 \times M \frac{A - B}{w} \quad (1)$$

where *A* is the volume (ml) of potassium hydroxide used to reach the neutral point, *B* is the volume (ml) corresponding to the blank titration, *M* is a molarity of potassium hydroxide solution (M) and *w* is the sample mass (g). Meanwhile, the percent of FFA (% FFA) was determined using Eq. 2:

$$\%\ \mathrm{FFA} = \frac{A - B}{w} \times M \times 28.2 \qquad (2)$$

where *A* is the volume (ml) of the titration solution, *B* is the volume (ml) of the blank, *M* is a molarity of the titration solution (M) and *w* is the sample mass (g); 28.2 indicated 10% of the oleic acid molecular weight.

3. Results and discussions

3.1. Stage 1: synthesis of SHER

3.1.1. The synthesis of precursor beads (NAD particles)

In the present work, porous precursor beads were synthesised by NAD polymerisation of VBC, St, PVP, Triton, BPO, ethanol (EtOH) and EGDMA. In this stage, the effect of monomer/comonomer concentration and the effect of cross-linker concentration were evaluated. The reaction scheme for the synthesis of precursor beads is presented in Fig. 1 (i.e. NAD polymerisation).

a) Effect of monomer/comonomer on the physicochemical properties of precursor beads

In the polymerisation reaction, a study on the effect of monomer concentration is an important element as it significantly effects the shape of the precursor beads and pore structure of the porous beads. Theoretically, the introduction of different concentrations of VBC in the monomer mixtures will result in the different level of chloromethyl groups. To investigate the effect of chloromethyl groups on the particle morphology, surface area and the chlorine content, a series of NAD precursor were synthesised at different St/VBC ratios. The recoveries of the precursor beads are considered good with more than 95% yield, and as shown in Table 1, the percentage of chlorine content obtained from the XRF analysis correlates well with the content of VBC in the monomer feed. Table 1 also shows that when the content of VBC (chloromethyl group) increases, the specific surface area of the precursor particles is also increased. The findings are in agreement with the findings from the study by Liu et al. [33] and Ahn et al. [34].

Table 1
Properties of precursor beads at different St/VBC concentrations measured by XRF and N_2 physisorption analysis.

Polymer type	Material sample code	Properties	SSA[a] ($m^2\ g^{-1}$)	Chlorine content (%)
Precursor	P 01	90% St/10% VBC	2	10.16
Precursor	P 02	80% St/20% VBC	4	12.83
Precursor	P 03	70% St/30% VBC	5	14.56
Precursor	P 04	60% St/40% VBC	7	16.67
Precursor	P 05	50% St/50% VBC	10	18.72

St, styrene; VBC, vinylbenzyl chloride; XRF, X-ray fluorescence.
[a] Specific surface area.

However, these particles are not monodispersed (Fig. 2). All samples (P01–P05) are found to be polydispersed, although the particles are in the micrometre size range. Nonetheless, low VBC concentration shows a better image of the precursor. A precursor with 20% of VBC (Fig. 2b) shows better uniformity in terms of shapes (i.e. spherical) than others. Besides that, there is no agglomeration of beads observed. The reduction of VBC fraction led to the low cross-linking degree and resulted in different pore structure. Thus, precursor particles at monomer/comonomer concentration of 80% St/20% VBC are selected for further experimental work.

b) Effect of cross-linker concentration on morphology and BET surface area of precursor beads

In theory, the pore structure is largely influenced by the content of the cross-linker. When the content of the cross-linker is lower or higher than a certain limit value, it will reduce the rigidity of the polymer beads and consequently contributes to the difficulty in maintaining their pore structure. In this study, EGDMA was used as a cross-linker to link the polymer chain. The effect of the cross-linker loading on the physical and chemical properties of the precursor beads was investigated, with different amounts of EGDMA (0.5, 0.7, 1.0, 1.3 and 1.5 wt%) introduced to the

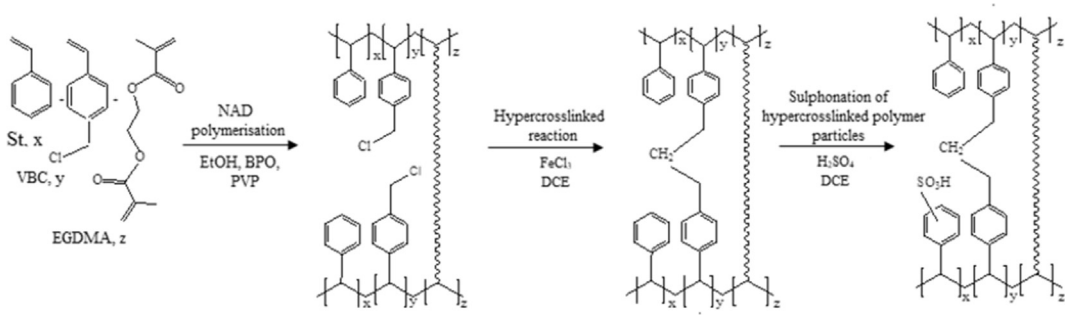

Fig. 1. Synthesis procedure for the sulphonated hypercrosslinked exchange resin (SHER). St, styrene; VBC, vinylbenzyl chloride; EGDMA, ethylene glycol dimethacrylate; NAD, nonaqueous dispersion; EtOH, ethanol; BPO, benzoyl peroxide; PVP, poly (*N*-vinylpyrrolidone); DCE, 1,2-dichloroethane.

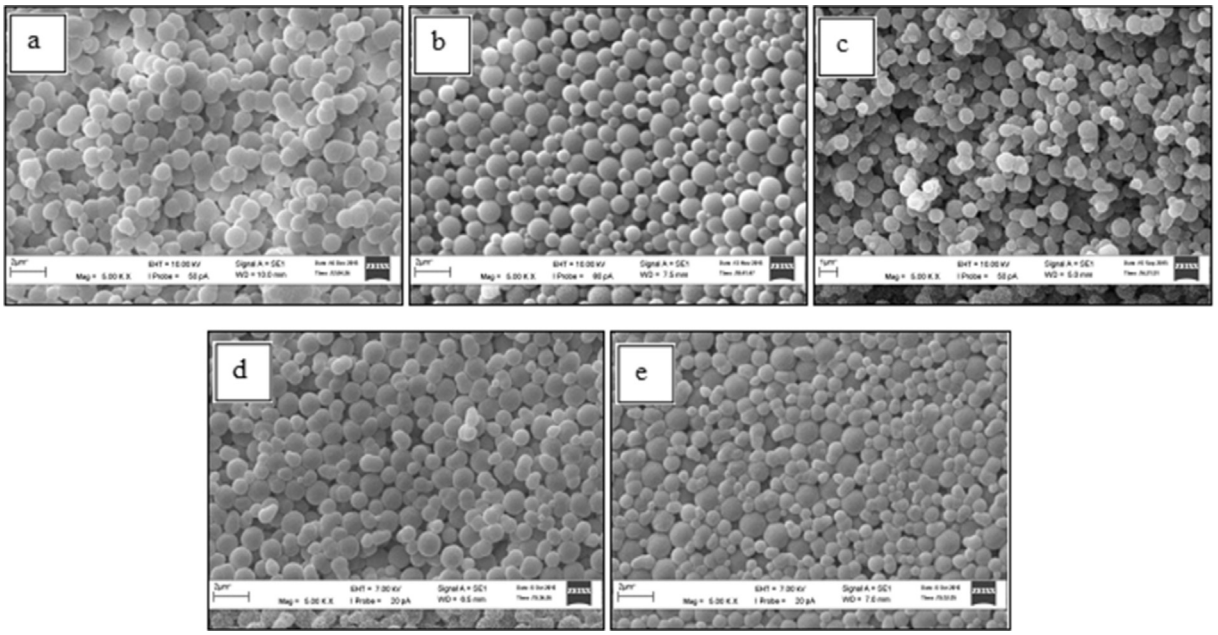

Fig. 2. SEM images (magnification, 5kX) of the precursor beads with different monomer/comonomer concentrations: (a) P01 – 90% St/10% VBC; (b) P02 – 80% St/20% VBC; (c) P03 – 70% St/30% VBC; (d) P04 – 60% St/40% VBC; (e) P05 – 50% St, 50% VBC. SEM, scanning electron microscopy; VBC, vinylbenzyl chloride.

precursor solution. The concentration of the monomer/comonomer was kept constant at 80% St/20% VBC. From the results, the increase of cross-linker loading simultaneously increases the specific surface area of the precursor particles (Table 2). This implies that the specific surface area of the beads is directly proportional to the cross-link density. According to Song and Winnik [35], when the cross-linker content increases, the number of pore increases, which simultaneously increases the specific surface area of the catalyst. At low cross-linker concentration, high mesopore and macropore formation takes place, resulting in low surface area. This is because, when the amount of cross-linker is low, the size of the micropores decreases and the micropores tend to be slightly fused. Besides that, high amount of the cross-linker will stabilise the precursor by making the pore structure stronger.

However, too low and too high amounts of EGDMA disturb the spherical structure of the precursor, as depicted in Fig. 3. When the amount of EGDMA is less than 0.7 wt% and more than 1.0 wt%, some of the precursor beads are unable to form good spherical shapes. Therefore, 1.0 wt% of EGDMA is selected as the optimum amount of the cross-linker needed as this amount is sufficient enough to hold the chain of the polymer structure while maintaining the pore structure and spherical shape of the beads.

Table 2
Properties of precursor beads at different EGDMA concentration.

Polymer type	Material sample code	Properties	SSA (m^2/g)
Precursor	P 06	0.5 wt % EGDMA	2.5
Precursor	P 07	0.7 wt % EGDMA	3
Precursor	P 08	1.0 wt % EGDMA	4
Precursor	P 09	1.3 wt % EGDMA	6
Precursor	P 10	1.5 wt % EGDMA	9

EGDMA, ethylene glycol dimethacrylate; SSA, specific surface area.

3.1.2. *Effect of Lewis acid catalyst on $FeCl_3$ on the physicochemical properties of hypercrosslinked beads*

A Lewis acid catalyst ($FeCl_3$) is introduced into the polymeric reaction to increase the surface area of the precursor beads by forming methylene bridges between aromatic groups and Lewis acid catalyst. The reaction between Lewis acid and aromatic groups creates pores within the resin. These bridges were built during the hypercrosslinking step via Friedel–Crafts reaction, and it led to the formation of highly porous polymer particles. Fig. 1 represents the reaction scheme for the synthesis of the hypercrosslinked beads (i.e. hypercrosslinked reaction).

To determine the effect of Lewis acid catalyst on the physical and chemical properties of the cross-linked precursor, ferric chloride and dichloroethane in different ratios ($FeCl_3$ to CH_2Cl) (i.e. 0.5:1, 1:1 and 1.5:1) were introduced to the cross-linked precursor solution. In this stage, the amount of the monomer, comonomer and cross-linker was kept constant, i.e., 80% St, 20% VBC and 1 wt% EGDMA, respectively. The beads were evaluated based on the physicochemical properties, i.e. XRF, surface morphology and porosity. Based on the XRF analysis (Table 3), the reduction in the percentage of chlorine content confirms the occurrence of the high level of cross-linking structure. This reaction involved the formation of multiple bridging between aromatic groups, as presented in Fig. 1. About 70–89% of Cl reduction is achieved by the precursor particles (Table 1). The finding is consistent with the finding from the study by Wang et al. [36]. The exploitation of the pendent chloromethyl groups via Lewis acid ($FeCl_3$) reaction yielded a good recovery of modified hypercrosslinked

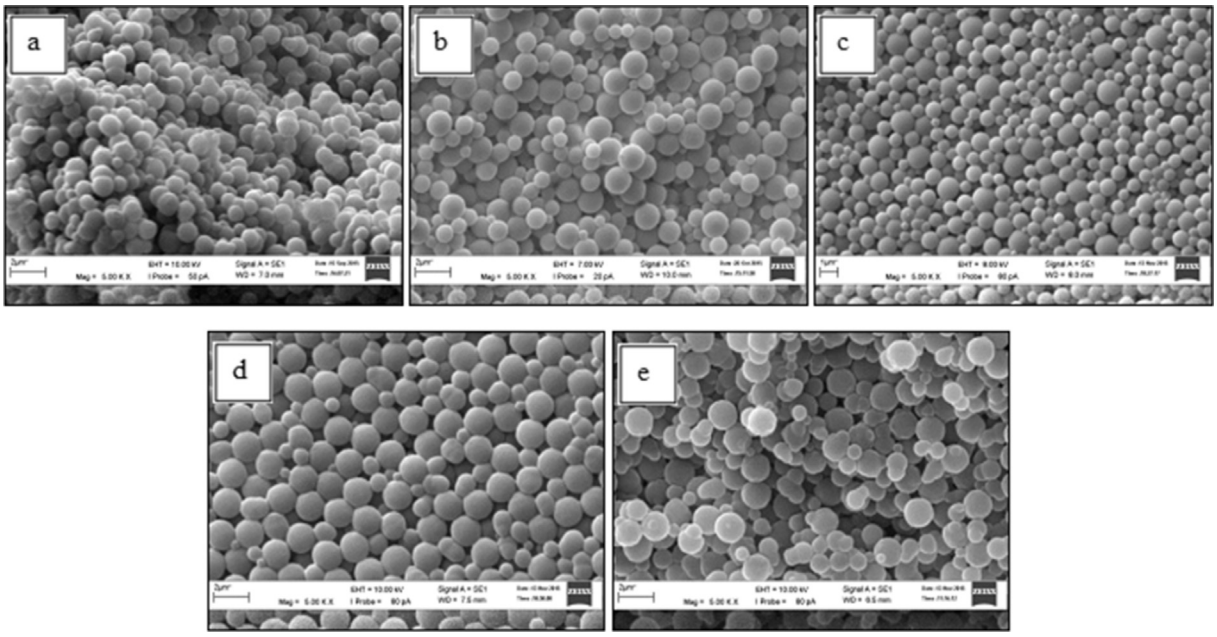

Fig. 3. SEM images (magnification, 5kX) of the precursor particles with different cross-linker concentrations: (a) P06 – 0.5 wt% EGDMA; (b) P07 – 0.7 wt% EGDMA; (c) P08 – 1 wt% EGDMA; (d) P09 – 1.3 wt% EGDMA; (e) P10 – 1.5 wt% EGDMA. EGDMA, ethylene glycol dimethacrylate; SEM, scanning electron microscopy.

Table 3
Properties of polymer beads.

Polymer type	Material sample code	Properties	SSA (m^2/g)	Chlorine content (%)
Hypercrosslinked polymer	MP 01	0.5:1 ($FeCl_3$:CH_2Cl)	456	5.67
Hypercrosslinked polymer	MP 02	1: 1 ($FeCl_3$:CH_2Cl)	698	2.12
Hypercrosslinked polymer	MP 03	1.5:1 ($FeCl_3$:CH_2Cl)	710	1.97

SSA, specific surface area.

particles. Based on the BET analysis, each sample shows a big increment in the specific surface area which clearly indicates the generation of highly porous particles. When the Friedel–Crafts reaction was introduced, the porosity of the beads increased. This is due to the formation of a large number of pores. Theoretically, a high molar ratio of $FeCl_3$ to CH_2Cl will increase the formation of methylene bridges. The increase of methylene bridges in the structure will contribute to high bead porosity, leading to the high specific surface area.

The SEM micrographs of hypercrosslinked beads are shown in Fig. 4. It is observed that the overall particle integrity is well retained, although the surface roughness is quite obvious. Fig. 4(b) of 1:1 ratio of $FeCl_3$ to CH_2Cl shows the best morphology in terms of uniformity of the spherical shape. From this image, the roughness of the surface, which represents the porosity of the surface, can be clearly seen. Higher molar ratio, i.e. 1.5:1 $FeCl_3$:CH_2Cl, results in agglomeration on the beads and changed the spherical shape of the resins. This is due to the excess amount of the Lewis acid catalyst used in the reaction, leaving the unreacted $FeCl_3$ on the surface of the beads. Thus, 1:1 molar ratio is chosen to be used in the sulphonation stage.

3.1.3. *Effect of the sulphonation reagent on the properties of SHER*

In this study, the sulphonation reagent, sulphuric acid (H_2SO_4), was introduced to the hypercrosslinked beads-solvent mixture at five different volumes, i.e. 1, 2, 3, 4 and 5 wt%. The amount of the monomer, comonomer, cross-linker and $FeCl_3$ used was kept constant at 80% St, 20% VBC, 1 wt% EGDMA and 1:1 molar ratio of $FeCl_3$:CH_2Cl. The synthesis procedure for the sulphonation of hypercrosslinked polymer beads is presented in Fig. 1. Table 4 summarises the results of the specific surface area and IEC of the SHER. From the result, it is found that the IEC increases with increasing H_2SO_4 concentration. This is due to the increment of SO_3H bonding on the particles. Based on the BET analysis, the specific surface area of the SHER increases when H_2SO_4 concentration increases from 1 to 4 wt %. However, the specific surface area decreases when 5 wt% of H_2SO_4 is added to the mixture. This is due to the blockage of the hypercrosslinked beads, resulting from the formation of the sulphur bridge, and this condition leads to a decrease in the specific surface area. Therefore, 4 wt% of H_2SO_4 (SHER 04) is taken as the best condition for the sulphonation of the hypercrosslinked polymer. The resins produced in this condition were used in the reaction process (i.e. esterification reaction).

3.2. *Catalyst characterisations*

All the catalysts were characterised by N_2 physisorption analysis, elemental analysis, IEC, TGA, FTIR spectroscopy

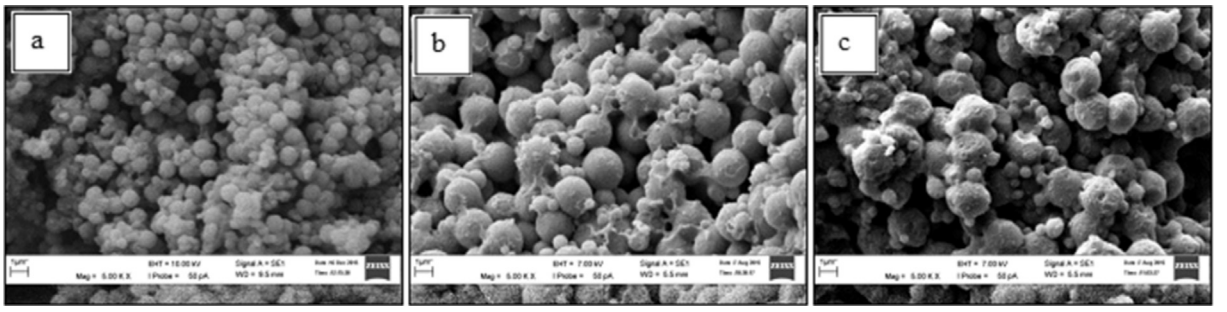

Fig. 4. SEM images (magnification, 5kX) of the polymer beads prepared by Friedel–Crafts reaction with different ratio of $FeCl_3$:CH_2Cl: (a) MP 01 – 0.5:1 ratio; (b) MP 02 – 1:1 ratio; (c) MP 0.3 – 1.5:1 ratio. SEM, scanning electron microscopy.

Table 4
Properties of sulphonated hypercrosslinked exchange resin (SHER).

Material Sample Code	Properties	SSA (m^2 g^{-1})	IEC (mmol g^{-1})
SHER 01	1 wt% of H_2SO_4	698	3.7
SHER 02	2 wt% of H_2SO_4	720	4.0
SHER 03	3 wt% of H_2SO_4	765	4.5
SHER 04	4 wt% of H_2SO_4	836	5.1
SHER 05	5 wt% of H_2SO_4	654	5.4

IEC, ion-exchange capacity; SSA, specific surface area.

and SEM analysis. Discussion on the FTIR analysis is provided in the Supplemental file.

Fig. 5 shows the TGA thermograms of SHER, RCP145H, PK228LH and SK1BH catalysts. SHER shows the highest decomposition point, followed by SK1BH, PK228LH and RCP145H. Three weight loss stages are observed in the TGA profile of SHER. The first one is located below 100 °C. This weight loss is attributed to the removal of the adsorbed water on the surface of the resin. SHER shows a very low decrement peak at this stage because of the inability of SHER to absorb more moisture compared with the other catalysts. This criterion was also proven by the FTIR analysis in the Supplemental file, where the result shows that the intensity of OH bond is very low. The second stage occurred between 398 and 450 °C, which is probably due to the decomposition of sulphonic groups of SHER [37–40]. The weight loss from 500 °C to 780 °C shows the destruction of the polymer. From the analysis, it is shown that SHER has a very good temperature resistance which is up to 398 °C. For the commercial catalysts (i.e. RCP145H, PK228LH and SK1BH), all the catalysts show the sulphonic decomposition point at approximately 250–300 °C.

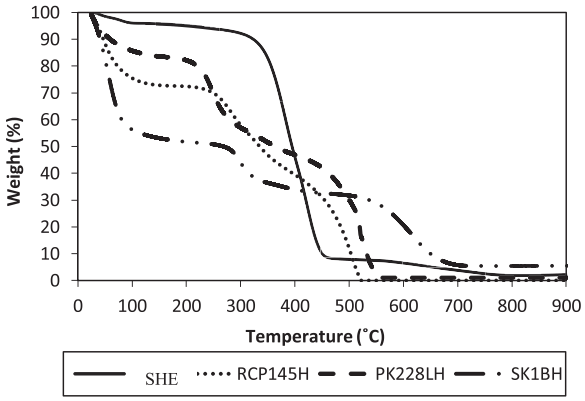

Fig. 5. Thermogravimetric curves of SHER, RCP145H, PK228LH and SK1BH catalyst. SHER, sulphonated hypercrosslinked exchange resin.

Fig. 6 represents the surface morphology of SHER, Diaion RCP145H, Diaion PK228LH and Diaion SK1BH. A porous structure of SHER can be seen in Fig. 6(a) resulted from the cross-linking activity during the synthesis process, which shows a rough surface of SHER with the presence of tiny holes. Fig. 6(b) and (c) show the morphologies of Diaion RCP145H and Diaion PK228LH, taken at 5kX magnification. Both catalysts show a quite similar surface morphology as SHER. According to the manufacturer (Mitsubishi Chemical Corporation), the catalysts are classified as highly porous and porous ones, respectively. In contrast, a smoother surface can be seen for the gelular resin (Fig. 6(d)) taken at 2kX magnification. The presence of pores within the catalyst structure was less significant than in the other three resins.

Specific surface area, average pore diameter and total pore volume for SHER, Diaion RCP145H and Diaion PK228LH are summarised in Table 5. The properties of SK1BH could not be analysed because of the low surface area (i.e. < 0.1 m^2 g^{-1}). SHER has the highest surface area which is 836 m^2 g^{-1}, followed by RCP145H (28.2 m^2 g^{-1}) and PK228LH (0.5 m^2 g^{-1}). SHER also shows the highest average pore diameter. Meanwhile, RCP145H shows the highest total pore volume, whereas PK228LH has the lowest surface area and average pore diameter. From the average pore diameter point of view, SHER can be classified as mesoporous, and RCP145H and PK228LH, as microporous.

The elemental analysis results for the resins are presented in Table 5. As confirmed by the manufacturer, all resins supplied by Mitsubishi Chemicals Corporation should only consist of carbon, hydrogen, sulphur and oxygen. The same goes for the self-synthesised resin, i.e. SHER, as none of the nitrogen bonding was formed during the polymerisation reaction. Table 5 shows the percentage of elements present in each resin. The considerable percentage of nitrogen present in the analysis data might be due to the contamination occurred during the analysis through the combustion process. Results from Table 5 show that

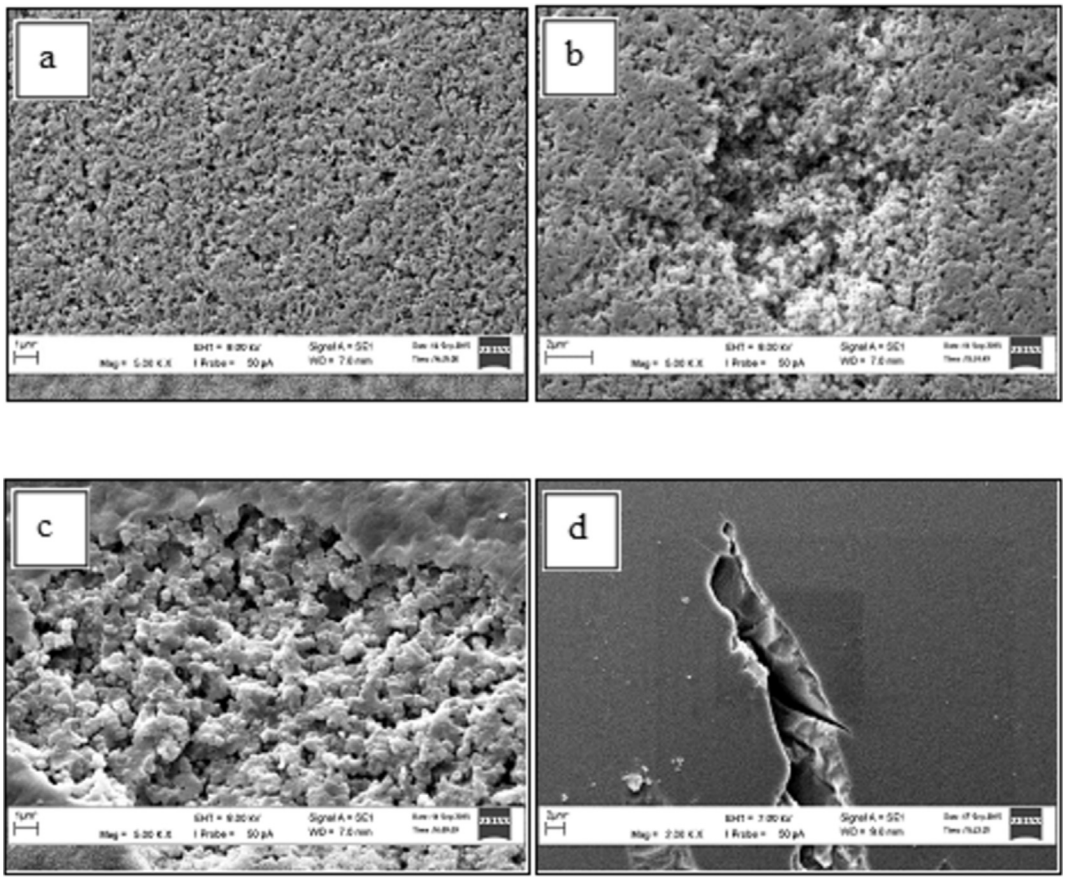

Fig. 6. SEM images of the ion-exchange catalyst resins: (a) SHER; (b) RCP145H; (c) PK228LH; (d) SK1BH. SEM, scanning electron microscopy; SHER, sulphonated hypercrosslinked exchange resin.

Table 5
Physical and chemical properties of SHER, Diaion RCP145H, Diaion PK228LH and Diaion SK1BH.

Catalyst properties	Materials			
	SHER	RCP145H	PK228LH	SK1BH
Physical appearance	Opaque spherical beads			
Functional group	*Sulphonic acids			
Polymer structure	Highly porous polystyrene cross-linked EGDMA	*Highly porous polystyrene cross-linked DVB	*Porous polystyrene cross-linked DVB	*Gelular polystyrene cross-linked DVB
Cross-linking level	Highly cross-linked	*Highly cross-linked	*Medium cross-linked	*Low cross-linked
Decomposition temperature (°C)	398	260	280	300
True density (g cm^{-1})	1.13	1.27	1.34	1.51
N_2 physisorption analysis				
BET surface area (m^2/g)	836	256	178	<0.1
Total pore volume (cm^3/g)	1.25	0.6	0.3	<0.1
Average pore diameter (nm)	21.2	18.8	16.6	<0.1
Elemental analysis				
Carbon content (%)	72.9	35.43	44.72	43.82
Hydrogen content (%)	6.23	6.44	7.90	6.59
Nitrogen content (%)	0.01	0.84	1.38	3.04
Sulphur content (%)	10.30	8.21	11.90	13.26
Particle size (μm)	3–450	400–1000	440–900	390–895
Ion-exchange capacity (mmol/g)	5.1	4.6	4.8	5.0

The information provided by Mitsubishi Chemical Corporation was denoted by (*) symbol; BET, Brunauer–Emmett–Teller; EGDMA, ethylene glycol dimethacrylate; SHER, sulphonated hypercrosslinked exchange resin; DVB, divinylbenzene.

SHER has the highest percentage of carbon (72.9%). This is probably resulted from the reaction activity during the synthesis process of SHER. Diaion PK228LH has the highest amount of hydrogen (7.9%), and Diaion SK1BH has the highest loading of sulphur element (13.26%). On the other hand, Diaion RCP145H has the least amount of carbon (35.43%) and sulphur (8.21%).

3.3. Stage 2: esterification of FFAs in SUCO using ion-exchange resins as a catalyst

In this section, the performance of SHER was compared with that of the commercial ion-exchange resins Diaion RCP145H, Diaion PK228LH and Diaion SK1BH. These four resins were selected because of their differences in structure and porosity. SHER and RCP145H are categorised as highly porous resins, PK228LH is categorised as a less porous resin and SK1BH is classified as a gelular resin. To identify the best catalysts for the esterification reaction, the same reaction conditions of 1.5 wt% of catalyst loading, 60 °C, 12:1 of methanol-to-SUCO feed molar ratio and 150 rpm were applied to each resin and used throughout the reaction. After 8 h, 90% of the FFA content was successfully converted to fatty acid methyl ester (FAME) using the SHER catalyst, and the FFA conversions for Diaion RCP145H, Diaion SK1BH and Diaion PK228LH are 85, 68 and 57%, respectively. The results are presented in Fig. 7.

This phenomenon can be explained by the physical and chemical properties of the resins obtained from the analysis of N_2 physisorption, PSD, acid capacity measurement and elemental composition. The high FFA conversion of SHER was possibly contributed by the large specific surface area and average pore diameter which created higher accessible active sites for the reaction.

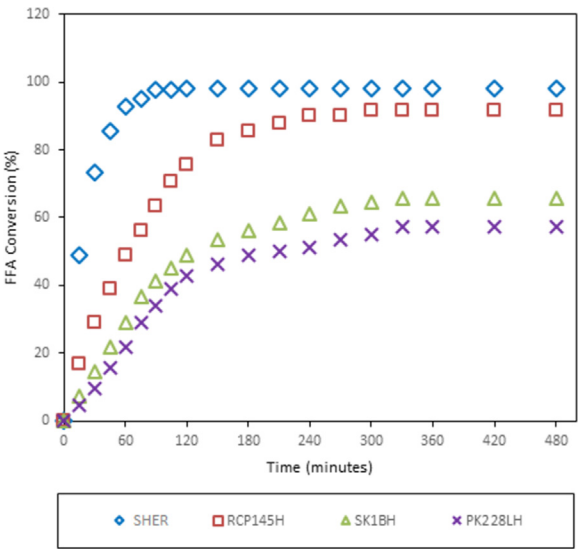

Fig. 7. Effect of diverse types of ion-exchange resins on FFA conversion (reaction conditions: 1.5 wt% of catalyst loading, 60 °C, 12:1 molar ratio of methanol to SUCO and 150 rpm of stirring speed). FFA, free fatty acid; SHER, sulphonated hypercrosslinked exchange resin; SUCO, simulated used cooking oil.

Furthermore, based on the PSD analysis (Table 5), SHER showed the smallest particle size compared with the other resins. Small particle size leads to a large external surface area, resulting in a fast reaction rate and simultaneously increased the FFA conversion. In addition, the sulphur content of SHER is relatively high, and this condition favours the esterification reaction. High sulphur content creates more active sites within the catalyst pores which contribute to high FFA conversion in a short reaction time (i.e. less than 120 min is needed to reach reaction equilibrium). Diaion RCP145H resin also gave high FFA conversion as compared with the other two Diaion resins (Diaion SK1BH and Diaion PK228LH). Even though it has the lowest sulphur content, the large total pore volume helps FFA to easily access the active sites of the catalyst because the active sites (i.e. sulphonic acid groups) are located close to the outer surface of the catalyst. The cross-linking degree also contributes to excellent conversion of FFAs. As shown in Fig. 7, highly cross-linked resins (SHER and Diaion RCP145H) give higher FFA conversion than low cross-linked resins (Diaion PK228LH and Diaion SK1BH). This is because highly cross-linked resins have a tougher matrix structure which helps to create a high resistance towards chemical and physical breakdown than low cross-linked resins. Meanwhile, SK1BH (gel-type resin) showed higher conversion than Diaion PK228LH (macroreticular resin). This might be due to the high acid capacity value of Diaion SK1BH (5.0 mmol g^{-1}) as compared with Diaion PK228LH (4.8 mmol g^{-1}), as shown in Table 5. Besides that, Diaion SK1BH possesses higher amount of sulphonic groups in their resin matrix than Diaion PK228LH (Table 5). These data also probably indicate that the number of the catalytic sites potentially accessible to oil was higher for the gelular resin Diaion SK1BH than for porous resin Diaion PK228LH.

4. Conclusion

In this work, the FFA esterification of acidified oil using self-synthesised and commercial ion-exchange resins as catalysts has been successfully carried out. In the first stage, SHER in the form of micrometre sized with spherical shape was successfully synthesised with the best conditions of 80%/20% monomer/comonomer concentration, 1.0 wt% cross-linker, 1:1 of $FeCl_3$:CH_2Cl molar ratio and 4 wt% sulphonation reagents. The specific surface area of 836.12 m^2 g^{-1} and decomposition point at 398 °C were successfully achieved at these conditions. High formation of methylene bridges during the hypercrosslinked reaction led to high specific surface area and thermal decomposition of SHER. The performance of self-synthesised SHER was compared with those of three commercial resins, namely, the Diaion RCP145H, Diaion PK228LH and Diaion SK1BH. In this stage, SHER gives the highest reduction of FFAs with more than 90% conversion at the condition of 1.5 wt% catalyst loading, 60 °C reaction temperature, 12:1 methanol-to-SUCO molar ratio and 150 rpm stirring speed. Owing to its high porosity, high specific surface area and accessible acid sites, the synthesised SHER exhibited better performance than Diaion RCP145H, PK228LH and SK1BH.

Acknowledgements

This work was supported by Universiti Malaysia Pahang [RDU 140357, RDU 130311, GRS 1403159] and the Ministry of Education, Malaysia for awarding the FRGS research grant vote FRGS/1/2014/TK04/UMP/02/5 (RDU140133). The authors would like to thank Mitsubishi Chemical Corporation for supplying the ion-exchange resins.

Appendix A. Supplementary data

Supplementary data to this article can be found online at https://doi.org/10.1016/j.crci.2019.08.004.

References

[1] S. Rafiei, S. Tangestaninejad, P. Horcajada, M. Moghadam, V. Mirkhani, I. Mohammadpoor-Baltork, R. Kardanpour, F. Zadehahmadi, Chem. Eng. J. 334 (2018) 1233–1241.
[2] L.A. Jermolovicius, L.C.M. Cantagesso, R.B. do Nascimento, E.R. de Castro, E.V. dos, S. Pouzada, J.T. Senise, Chem. Eng. Process 122 (2017) 380–388.
[3] E.H.S. Moecke, R. Feller, H.A. dos Santos, M. de Medeiros Mechado, A.L.V. Cubas, A.R. de Aguiar Dutra, L.L.V. Santos, S.R. Soares, J. Clean. Prod. 135 (2016) 679–688.
[4] S. Pleanjai, S.H. Gheewala, S. Garivait, J. Clean. Prod. 17 (2009) 873–876.
[5] S. Banerjee, S. Rout, S. Banerjee, A. Atta, D. Das, Energy Convers. Manag. 195 (2019) 844–853.
[6] Z. Ullah, M.A. Bustam, Z. Man, A.S. Khan, N. Muhammad, A. Sarwono, Renew. Energy 114 (2017) 755–765.
[7] F.J. Gutiérrez Ortiz, P. de Santa-Ana, J. Supercrit. Fluids 128 (2017) 349–358.
[8] L.F. Chuah, S. Yusup, A.R.A. Aziz, A. Bokhari, M.Z.J. Abdullah, J. Clean. Prod. 112 (2016) 4505–4514.
[9] Z. Ullah, M.A. Bustam, Z. Man, Renew. Energy 77 (2015) 521–526.
[10] O. Aboelazayem, M. Gadalla, B. Saha, Renew. Energy 143 (2019) 77–90.
[11] S. Saeidi, P. Jouybanpour, A. Mirvakilli, D. Iranshahi, J.J.J. Klemeś, Clean. Prod. 136 (2016) 23–30.
[12] A.A. de Jesus, D.F. de Santana Souza, J.A. de Oliveira, M.S. de Deus, M.G. daSilva, E. Franceschi, S.M. da Silva Egues, C. Dariva, Energy Convers. Manag. 171 (2018) 1679–1703.
[13] N. Boz, N. Degirmenbasi, D.M. Kalyon, Appl. Catal. B Environ. 165 (2015) 723–730.
[14] S. Gan, H.K. Ng, C.W. Ooi, N.O. Motala, M.A.F. Ismail, Bioresour. Technol. 101 (2010) 7338–7343.
[15] R. Suresh, J.V. Antony, R. Vengalil, G.E. Kochimoolayil, R. Joseph, Ind. Crop. Prod. 95 (2017) 66–74.
[16] F.H. Cao, Y. Chen, F.Y. Zhai, J. Li, Biotechnol. Bioeng. 101 (2008) 93–100.
[17] A.A. Costa, P.R.S. Braga, J.L. de Macedo, J.A. Dias, S.C. L Dias, Microporous Mesoporous Mater. 147 (2012) 142–148.
[18] Y. Duan, Y. Wu, Y. Shi, M. Yang, M. Zhang, Q. Zhang, H. Hu, Catal. Commun. 82 (2016) 32–35.
[19] J. Fu, L. Chen, P. Lv, L. Yang, Z. Yuan, Fuel 154 (2015) 1–8.
[20] Y. Jiang, X. Li, H. Zhao, Z. Hou, Fuel 255 (2019) 115842.
[21] S.M. Silva, A.F. Peixoto, C. Freire, Renew. Energy 146 (2020) 2416–2429.
[22] V.M. de Aguiar, A.L. de Souza, F.S. Galdino, M.M.C. da Silva, V.G. Teixeira, E.R. Lachter, Renew. Energy 114 (2017) 725–732.
[23] D.C. Boffito, C. Pirola, F. Galli, A. Di Michele, C.L. Bianchi, Fuel 108 (2013) 612–619.
[24] N. Boz, N. Degirmenbasi, D.M. Kalyon, Appl. Catal. B Environ. 165 (2015) 723–730.
[25] J.Y. Park, D.K. Kim, J.S. Lee, Bioresour. Technol. 101 (2010) 62–65.
[26] Y. Feng, B. He, Y. Cao, J. Li, M. Liu, F. Yan, X. Liang, Bioresour. Technol. 101 (2010) 1518–1521.
[27] S. Furuta, H. Matsuhashi, H.,K. Arata, Catal. Commun. 5 (2004) 721–723.
[28] M. Tariq, S. Ali, N. Khalid, Renew. Sustain. Energy Rev. 16 (2012) (2012) 6303–6316.
[29] L. Shao, J. Huang, J. Colloid Interface Sci. 507 (2017) 42–50.
[30] L. Shao, Y. Li, T. Zhang, M. Liu, J. Huang, Ind. Eng. Chem. Res. 56 (2017) 2984–2992.
[31] T. Zhang, F. Zhou, J. Huang, R. Man, Chem. Eng. J. 339 (2018) 278–287.
[32] V. Davankov, M. Tsyurupa, M. Ilvin, L. Pavlova, J. Chromatogr. A 965 (2002) 65–73.
[33] Q.Q. Liu, L. Wang, A.G. Xiao, H.J. Yu, Q. Tan, Eur. Polym. J. 44 (2008) 2516–2522.
[34] J.H. Ahn, J.E. Jang, C.G. Oh, S.K. Ihm, J. Cortez, D.C. Sherrington, Macromolecules 39 (2006) 627–632.
[35] J. Song, M.A. Winnik, Macromolecules 38 (2005) 8300–8307.
[36] X. Wang, K. Dai, L. Chen, J. Huang, Y.N. Liu, Chem. Eng. J. 242 (2014) 19–26.
[37] S.S. Viera, I. Graça, A. Fernandes, F.M. José Manuel, M.F. Ribeiro, Z.M. Magriotis, Microporous Mesoporous Mater. 270 (2018) 189–199.
[38] L. Noda, R. de Almeida, L.F. Probst, N. Goncalves, J. Mol. Catal. 225 (2005) 39–46.
[39] B. Lu, Z. wu, L. Ma, X. Yuan, J. Taiwan Inst. Chem. Eng. 88 (2018) 1–7.
[40] K. Malins, J. Brinks, V. Kampars, I. Malina, Appl. Catal., A 519 (2016) 99–106.